catalysts

MDPI

Article

Performance and Mechanism of $Fe_{80}P_{13}C_7$ Metal Glass in Catalytic Degradation of Methylene Blue

Li Ma [1], Kun Zhang [2,*], Feilong Guo [2] and Tiejun Kuang [2]

[1] School of Emergency Management and Safety Engineering, China University of Mining and Technology-Beijing, Beijing 100083, China; ma3442811943@163.com
[2] Jinneng Holding Coal Industry Group, Datong 037001, China; feilong1332025@163.com (F.G.); tiejun133025@163.com (T.K.)
* Correspondence: tb20020037b4@cumt.edu.cn; Tel.: +86-131-6027-5662

Abstract

This study systematically investigates the catalytic degradation performance and reaction mechanism of $Fe_{80}P_{13}C_7$ Metal Glass (MG) in a Fenton-like system for the removal of Methylene Blue (MB). Kinetic experiments on degradation reveal that under acidic conditions (pH = 3), $Fe_{80}P_{13}C_7$ MG exhibits exceptional catalytic activity, achieving complete degradation of a 50 mg/L MB solution within 12 min. Its degradation rate significantly surpasses that of $Fe_{78}Si_9B_{13}$ MG and commercially available ZVI powder. Key parameters such as catalyst dosage, H_2O_2 concentration, solution pH, and initial dye concentration were systematically examined to determine the optimal reaction conditions. The characterization results indicate that $Fe_{80}P_{13}C_7$ MG maintains high activity even after multiple cycles of use, attributed to surface selective corrosion and crack formation during the reaction process. This "self-renewal" mechanism continuously exposes fresh active sites. Mechanistic studies confirm that the degradation process is driven by an efficient redox cycle between Fe^{2+}/Fe^{3+} within the material, ensuring sustained and stable generation of •OH, which ultimately leads to the complete mineralization of MB molecules. This research provides solid experimental and theoretical foundations for the application of $Fe_{80}P_{13}C_7$ MG in dye wastewater treatment.

Keywords: metal glass; azo dye; efficient recycling; degradation; advanced oxidation processes

check for updates

Academic Editor: Enric Brillas

Received: 15 October 2025
Revised: 6 November 2025
Accepted: 20 November 2025
Published: 10 December 2025

Citation: Ma, L.; Zhang, K.; Guo, F.; Kuang, T. Performance and Mechanism of $Fe_{80}P_{13}C_7$ Metal Glass in Catalytic Degradation of Methylene Blue. *Catalysts* **2025**, *15*, 1158. https://doi.org/10.3390/catal15121158

Copyright: © 2025 by the authors. Licensee MDPI, Basel, Switzerland. This article is an open access article distributed under the terms and conditions of the Creative Commons Attribution (CC BY) license (https://creativecommons.org/licenses/by/4.0/).

1. Introduction

The textile dyeing and finishing industry wastewater is one of the major sources of industrial wastewater globally. With the rapid advancement of technology worldwide, there has been a significant increase in dyeing wastewater alongside the implementation of automation technologies aimed at enhancing operational efficiency within this sector. This growing volume of dyeing wastewater has gradually attracted widespread attention [1,2]. As a common type of industrial effluent, dyeing wastewater poses severe threats to the natural environment, particularly aquatic ecosystems. Due to its toxicity, resistance to degradation, and large production volumes, it has been extensively studied as a primary source of industrial wastewater [3,4].

Common treatment methods for textile dyeing and finishing industry wastewater include physical adsorption [5,6], membrane separation [7–9], biological treatment [10–12], redox processes [13,14], and zero-valent metals [15,16]. However, these methods often

involve relatively complex operations and require considerable human resources, which limits the development of effective wastewater treatment solutions. Therefore, it is imperative to continuously explore advanced new materials and innovative methodologies for degrading textile dyeing wastewaters effectively.

In recent years, it has been observed that metal glasses (MGs) exhibit remarkable catalytic degradation capabilities for dye wastewater due to their thermodynamic metastability, high surface residual stress, and significant number of unsaturated sites [17,18]. Currently, the primary types of MGs used in the catalytic degradation of dye wastewater include Mg-based [19–22], Al-based [23–27], Co-based [28,29], and Fe-based [30–33] thin strips, fine powders, and nanoporous structures. These materials have been demonstrated to possess excellent catalytic degradation performance for dyes. Among them, Fe-based MGs not only exhibit outstanding soft magnetic properties and oxidation characteristics, but also offer advantages in practical applications such as low cost, ease of preparation, and convenient recovery [34]. Consequently, Fe-based MGs are regarded by scholars, both domestically and internationally, as the most promising catalysts for the catalytic degradation of dye wastewater [35,36].

Currently, the most researched Fe-based MGs for catalyzing the degradation of dye wastewater are from the Fe-Si-B system or Fe-Si-B based alloys with additional elements. This is due to their excellent ability to form an amorphous structure and the tendency to develop a loose surface layer that facilitates electron transfer [37]. Zhang et al. investigated the catalytic degradation of 3,5-dichlorosalicylic acid using both amorphous and crystalline forms of $Fe_{78}Si_9B_{13}$ under neutral conditions [38]. Professor Haifeng Zhang and colleagues added sodium persulfate to the $Fe_{78}Si_8B_{14}$ amorphous alloy, achieving a 99% degradation rate for Acid Orange II within 8 min. They proposed two coexisting degradation mechanisms [39]: the reductive degradation by organic small molecules and Fe^{2+} products, and the oxidative degradation by $SO_4^{-}\bullet$ generated from the activation of sodium persulfate. The results indicated that the degradation rate was significantly faster for the amorphous form compared to its crystalline counterpart.

While Fe-based MGs (e.g., the Fe-Si-B system) have demonstrated excellent Fenton-like catalytic activity, current research remains predominantly focused on these established alloy systems. In contrast, although the Fe-P-C system is renowned for its exceptional glass-forming ability and cost-effectiveness, it has received comparatively limited attention in the field of advanced oxidation processes. In this study, we report the catalytic degradation of MB using $Fe_{80}P_{13}C_7$ amorphous strips via a Fenton-like process. For comparison, the degradation performance of industrial zero-valent iron (ZVI) powder was also investigated. The results demonstrate that the $Fe_{80}P_{13}C_7$ strips achieve significantly higher degradation efficiencies compared to the ZVI powder. During cyclic testing, the self-renewal behavior of the strips, coupled with the continuous generation of •OH through the Fe^{2+}/Fe^{3+} redox cycle in the MB solution, enables sustained catalytic activity. This work develops an intrinsically highly reactive amorphous alloy catalyst capable of driving Fenton-like reactions efficiently and cost-effectively, demonstrating great potential for enabling simplified and sustained cyclic degradation processes.

2. Results and Discussion

2.1. Degradation Properties of $Fe_{80}P_{13}C_7$ MG

To evaluate the degradation performance of $Fe_{80}P_{13}C_7$ MG on MB, this study conducted systematic tests from two perspectives: degradation kinetics and cyclic stability. Figure 1a illustrates the changes in ultraviolet-visible absorption spectra during the catalytic degradation process of MB using $Fe_{80}P_{13}C_7$ MG in a solution with an initial concentration of 50 mg/L. The experiments were carried out under controlled conditions, specifically at a

constant temperature of 25 °C, pH = 3, and H_2O_2 concentration of 5 mmol/L. As shown in the figure, this material exhibits excellent catalytic activity: after just 6 min, the degradation rate of MB exceeds 85%; nearly complete degradation is achieved within 9 min; and total removal occurs by the end of 12 min. To determine the activation energy for the catalytic degradation of MB by $Fe_{80}P_{13}C_7$, we conducted kinetic tests at various temperatures (25 °C, 35 °C, 45 °C, and 55 °C). The results are presented in Figure 1b. Within the temperature range of 25 °C to 55 °C, the degradation rate significantly increased with rising temperature. Under conditions of 25 °C, MB was nearly completely degraded within 12 min; when the temperature was raised to 35 °C and then to 45 °C, the degradation process was shortened to just 9 min. Further increasing the temperature to 55 °C allowed for complete degradation of MB in only 6 min. According to Arrhenius equation calculations [40], the apparent activation energy for this degradation reaction is approximately 18.22 kJ/mol, which is lower than that reported for most Fenton-like catalysts. This indicates that $Fe_{80}P_{13}C_7$ exhibits superior catalytic activity and more readily triggered reaction kinetics characteristics. To evaluate the cyclic stability of $Fe_{80}P_{13}C_7$ MG, we conducted a series of ten consecutive degradation experiments using MB. The results are presented in Figure 1c,d. Figure 1c shows the C_t/C_0 curve, which indicates a slight increase in the time required for complete degradation of MB as the number of cycles increases. Figure 1d demonstrates that while the apparent k_{obs} fluctuates around 0.5 min^{-1}, it exhibits a downward trend over time. Notably, after 11 min of reaction, the degradation rate consistently remains at approximately 95%, ultimately stabilizing above 90%. These findings suggest that although there is a decline in catalytic activity during repeated use, $Fe_{80}P_{13}C_7$ MGs maintain an efficiency exceeding 90% relative to its initial value, thereby exhibiting commendable cyclic stability.

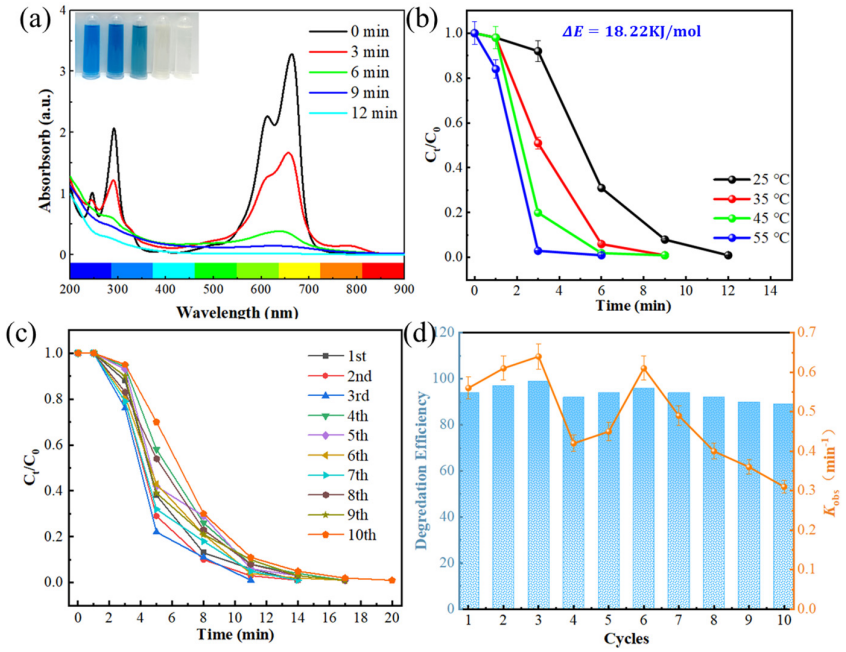


Figure 1. (**a**) The ultraviolet spectrum of the $Fe_{80}P_{13}C_7$ MG as it degrades MB, (**b**) the C_t/C_0 graph at different temperatures, (**c**) the C_t/C_0 graph of cyclic degradation, (**d**) the reaction rate constant of each cycle of degradation and the degradation efficiency at 11 min.

To objectively and comprehensively evaluate the performance advantages of $Fe_{80}P_{13}C_7$ catalysts, this study designed a systematic comparative experiment, conducting parallel comparisons with typical Fe-based MG ($Fe_{78}Si_9B_{13}$) and widely used commercial ZVI powder. The degradation kinetics curves of MB for the three catalysts under strictly controlled identical reaction conditions (including temperature, pH value, catalyst dosage,

and H_2O_2 concentration) are illustrated in Figure 2. Quantitative analysis indicates that the catalytic activity of $Fe_{80}P_{13}C_7$ significantly surpasses that of commercial ZVI powder while also demonstrating certain advantages over $Fe_{78}Si_9B_{13}$. This preliminary finding confirms its potential as a novel amorphous catalyst.

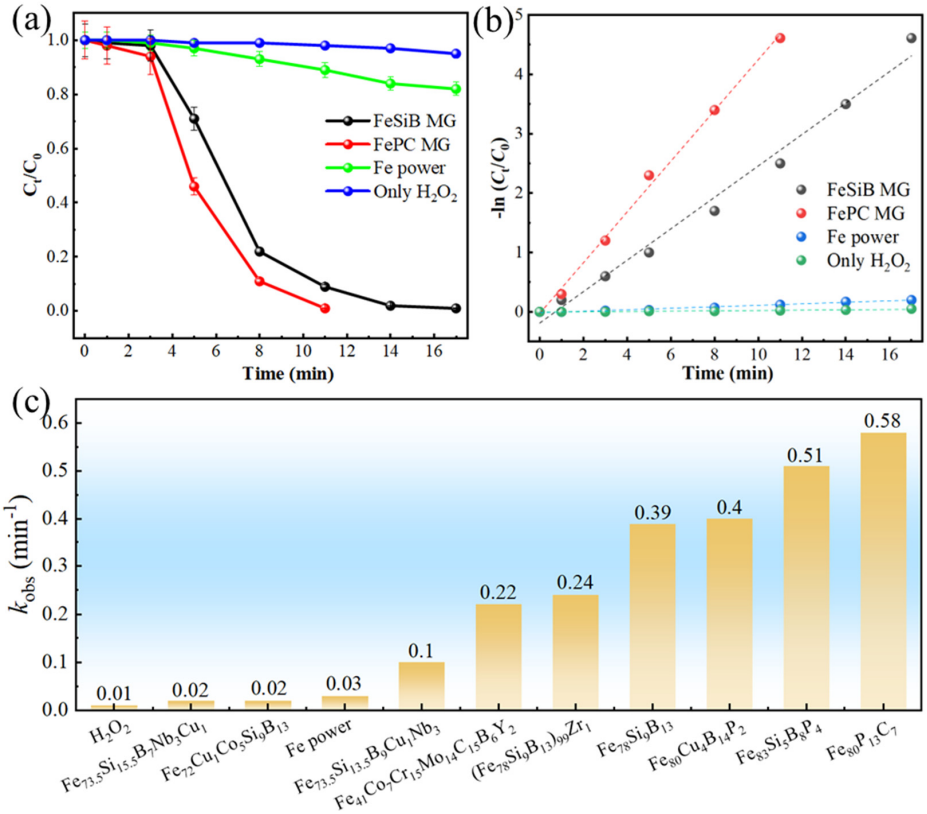


Figure 2. The (**a**) C_t/C_0 plots and (**b**) ln k curves of the catalytic degradation of MB by $Fe_{78}Si_9B_{13}$, $Fe_{80}P_{13}C_7$, Fe power and H_2O_2, (**c**) Comparison of k_{obs} for the degradation of azo dyes by different types of Fenton catalysts.

To ensure the rigor of our experimental conclusions, we established a blank control group without any catalyst (only adding H_2O_2). In this group, there was almost no degradation of MB, effectively ruling out any contribution from H_2O_2 self-decomposition to the overall degradation effect. This result substantiates that the degradation reaction is fundamentally driven by •OH generated through catalyst activation of H_2O_2. All kinetic experiments (presented in Figures 1b,d and 2a) were performed in triplicate (n = 3). The data points in the degradation profiles and the derived rate constants represent the mean value, and the error bars represent the standard deviation from these three independent experiments. This allows for a direct visual assessment of the reproducibility and variability of the data.

Furthermore, to position $Fe_{80}P_{13}C_7$'s performance within a broader context, we calculated its apparent k_{obs} and conducted a lateral comparison with various advanced Fe-based amorphous catalysts reported in the literature over the past five years [13–16,41–45]. The data reveal that $Fe_{80}P_{13}C_7$'s k_{obs} value ranks among the highest within similar materials. This finding not only robustly demonstrates $Fe_{80}P_{13}C_7$'s exceptional catalytic degradation capability but also highlights its competitive potential and application value in next-generation water treatment catalysis.

In the actual degradation process, the catalytic efficiency is influenced by various environmental factors, including dye concentration, catalyst dosage, H_2O_2 concentration, and solution pH. To investigate their specific effects, we first varied the concentration of

MB while keeping other conditions constant (catalyst at 1 g/L, pH 3, H_2O_2 at 5 mM, and temperature at 25 °C). As shown in Figure 3a, an increase in MB concentration significantly slows down the degradation efficiency. Subsequently, with a fixed MB concentration of 50 mg/L, we examined the impact of catalyst dosage. Figure 3b indicates that within the range of 0–2 g/L, the degradation rate increases with higher catalyst dosages. The solution pH is another critical factor; its influence is illustrated in Figure 3c: under acidic conditions (pH ranging from 2 to 5), the degradation rate initially rises before declining and reaches its peak at pH 3. In contrast, under neutral (pH 7) or alkaline (pH 9) conditions, catalytic degradation is almost completely inhibited. The above results demonstrate that this catalytic system can only exhibit high-efficiency degradation in an acidic environment. The significantly enhanced degradation efficiency observed at acidic pH can be attributed to multiple factors. Firstly, an acidic environment prevents the formation of inactive iron (oxy)hydroxide precipitates on the catalyst surface, thereby preserving the active sites. Secondly, the activation of H_2O_2 by iron species and the subsequent Fe (III)/Fe (II) redox cycle are known to be more favorable in acidic media [26]. Lastly, the scavenging of sulfate radicals by hydroxyl ions, which becomes pronounced at alkaline pH, is effectively suppressed. H_2O_2, as a precursor of free radicals, plays a crucial role in the degradation kinetics, with its concentration significantly influencing the process. As illustrated in Figure 3d, under fixed conditions for other variables, the degradation rate initially increases and then decreases with rising H_2O_2 concentrations, peaking at 5 mM. This nonlinear relationship typically arises from the dual role of H_2O_2 in reactions: at optimal levels, it serves as a source of free radicals that enhance degradation; however, when present in excess, it may quench free radicals and consequently reduce catalytic efficiency. This indicates that there exists an optimal dosage of H_2O_2 for this reaction. These results demonstrate that the process is dominated by catalytic oxidation rather than adsorption or photolysis.

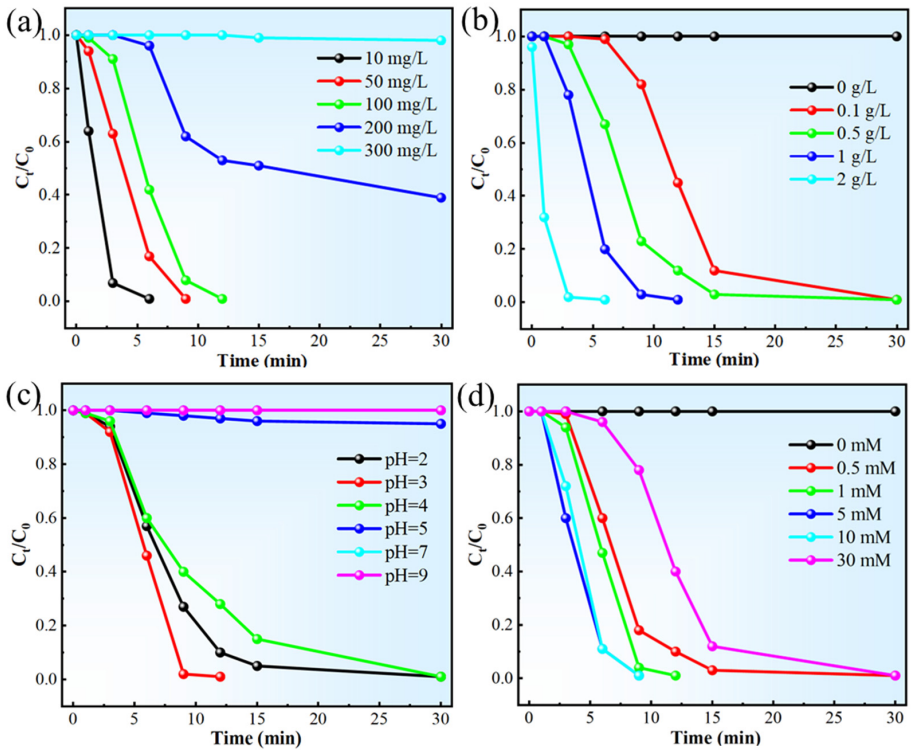


Figure 3. The effects of different (**a**) dye concentrations, (**b**) catalyst dosages, (**c**) pH values, and (**d**) H_2O_2 concentrations on the catalytic degradation efficiency of MB by $Fe_{80}P_{13}C_7$.

2.2. Mechanism Analysis of $Fe_{80}P_{13}C_7$ Catalytic Degradation of MB

To elucidate the evolution of surface morphology and its impact on catalytic performance during the cyclic degradation process of $Fe_{80}P_{13}C_7$ catalysts, this study systematically characterized the microstructural changes in the material in its initial state, after one cycle, and after ten cycles using scanning electron microscopy (SEM).

As shown in Figure 4a, the surface of the initial $Fe_{80}P_{13}C_7$ strips is smooth and uniform, exhibiting a typical homogeneous structure characteristic of MGs. However, after undergoing one degradation cycle (Figure 4b,c), significant alterations in surface morphology are observed: distinct striped deposits appear alongside the formation of small pores. These features are indicative of selective corrosion occurring within the MGs, where chemically active amorphous phases preferentially dissolve. This corrosion process significantly increases the specific surface area at a microscopic level and essentially exposes fresh active sites that have not been passivated. Consequently, this provides improved contact interfaces and reaction pathways for reactant molecules, which may be an important structural reason for the enhanced catalytic activity during early cycles.

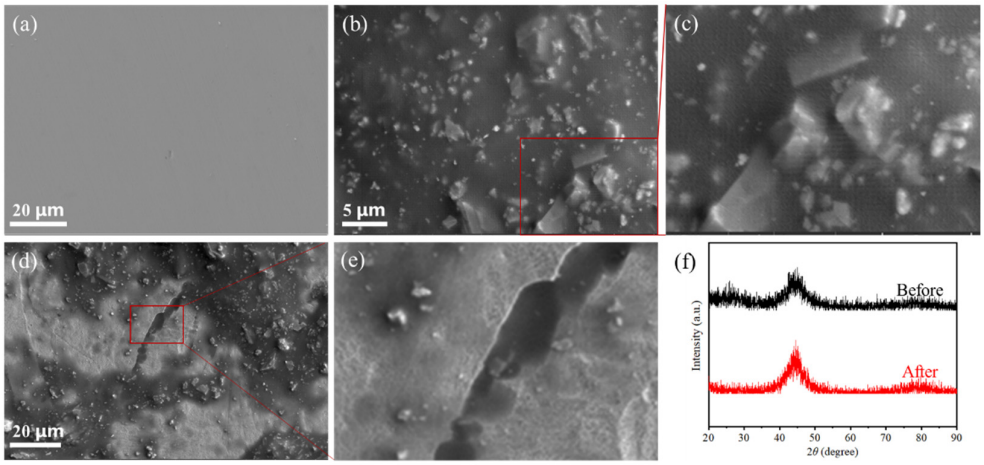


Figure 4. (**a**) SEM images of the catalyst surface before degradation, (**b**,**c**) SEM images of the catalyst surface after one cycle, (**d**,**e**) SEM images of the catalyst surface after 10 cycles, (**f**) XRD pattern of the catalyst surface before degradation.

With an increase to ten cycles (Figure 4d,e), further evolution occurs in the material's surface state: macroscopic cracks become clearly visible, resulting in a markedly roughened overall surface covered by a denser layer of particulate corrosion deposits. Notably, the emergence of these cracks is crucial for enabling $Fe_{80}P_{13}C_7$ to achieve multiple effective cyclic degradations. In harsh chemical environments akin to Fenton reactions, oxidation gradually occurs at the material's outer layer forming a passivation layer. Under reactive stress conditions, this passivation layer fractures continuously shedding off layers to expose underlying surfaces with high catalytic activity. This "surface peeling-internal renewal" self-renewal mechanism allows for sustained replenishment of active sites despite significant degradation in surface morphology over prolonged cycling periods and thus maintaining its efficacy in long-term degradation processes. Furthermore, we characterized the pristine $Fe_{80}P_{13}C_7$ sample using XRD, and the result is presented in Figure 4f. The XRD pattern displays a typical broad halo centered at approximately $2\theta = 44^\circ$, which is characteristic of an amorphous structure. The absence of sharp diffraction peaks confirms the fully amorphous nature of the $Fe_{80}P_{13}C_7$ ribbon.

It is important to note a limitation of this study. The characterization of the catalyst primarily relied on SEM and XRD. While our kinetic studies and scavenger experiments provide strong evidence for a radical-based mechanism, a more profound understanding

of the surface chemical states and structural stability would require advanced techniques such as XPS. Therefore, a systematic post-reaction characterization of structurally identical MGs will be a primary focus of our future investigations to unravel the detailed catalytic mechanism.

In order to elucidate the source of the remarkable catalytic activity of $Fe_{80}P_{13}C_7$, comparative experiments were conducted to investigate the contribution of specific active species to degradation performance. In classical Fenton-like reactions, •OH and $•O^{2-}$ are considered key reactive species for the degradation of azo dyes. Therefore, to distinguish the individual roles of •OH and $•O^{2-}$ in the degradation of MB, isopropanol (TBA, 10 mM) and para-benzoquinone (pBQ, 10 mM) were employed as scavengers for •OH and $•O^{2-}$, respectively, during the degradation experiments. As shown in Figure 5a, upon addition of TBA (•OH scavenger), a significant reduction in the degradation efficiency of $Fe_{80}P_{13}C_7$ was observed; conversely, when pBQ ($•O^{2-}$ scavenger) was added, only a slight decrease in degradation efficiency occurred. This indicates that the •OH present in solution is the primary active species contributing significantly to the degradation process.

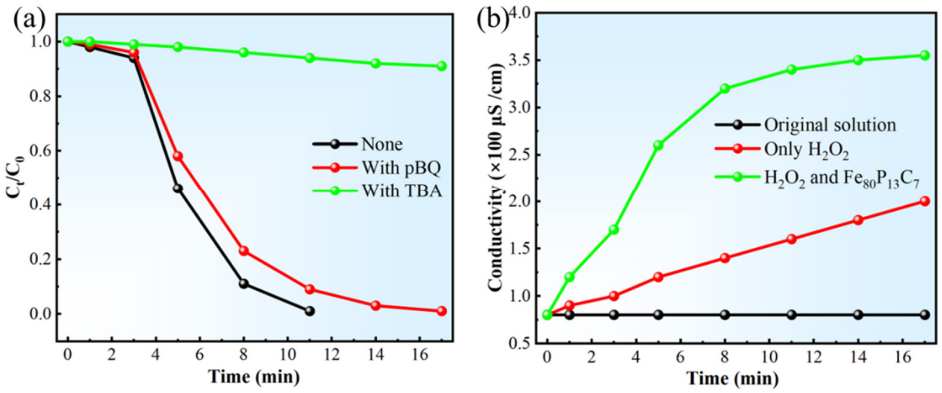


Figure 5. (**a**) Comparison of degradation efficiency with the addition of TBA and pBQ separately and with no addition. (**b**) Comparison of electrical conductivity of the original solution, only H_2O_2, and H_2O_2 and $Fe_{80}P_{13}C_7$.

To track the degradation process from the perspective of ionic concentration in solution, we measured the changes in electrical conductivity during the reaction for three systems: the initial MB solution, a system with only H_2O_2 added, and a system with both H_2O_2 and $Fe_{80}P_{13}C_7$ catalyst. The results are shown in Figure 5b.

Throughout the observation period, the electrical conductivity of the initial MB solution remained relatively constant, indicating that its composition was stable. In contrast, the system with only H_2O_2 exhibited a gradual increase in conductivity, which may be attributed to slight decomposition of H_2O_2 and limited oxidation of the dye. A stark contrast was observed in the system containing $Fe_{80}P_{13}C_7$ catalyst; here, conductivity significantly increased at early stages of reaction before gradually stabilizing. This trend clearly reveals the kinetics of the degradation reactions: The rapid rise in conductivity corresponds to an abundance of highly reactive free radicals generated by $Fe_{80}P_{13}C_7$-catalyzed decomposition of H_2O_2, facilitating reactions such as ring-opening and chain scission within MB molecules. This leads to substantial production of small molecular acids and inorganic ions that serve as conductive intermediates. As the reaction progresses into later stages and conductivity levels off, it indicates that MB has been largely mineralized and that types and concentrations of ions within the solution have reached dynamic equilibrium. These findings directly confirm that the $Fe_{80}P_{13}C_7$ catalyst effectively mineralizes MB molecules into inorganic ions such as CO_2, H_2O, NO_3^-, SO_4^{2-} etc., thereby achieving complete removal of pollutants.

Based on the aforementioned characterization and analysis of the microstructure, we speculate on the possible mechanism through which the $Fe_{80}P_{13}C_7$ degrades MB, as illustrated in Figure 6. Under acidic conditions, Fe^0 on the catalyst surface loses electrons and is converted to Fe^{2+}, establishing a typical Fenton-like system with H_2O_2 [37,38]. The interaction between H_2O_2 and Fe^{2+} generates •OH [40,41]. These •OH radicals possess strong oxidative properties, enabling them to oxidize MB molecules into harmless inorganic small molecules such as CO_2 and H_2O.

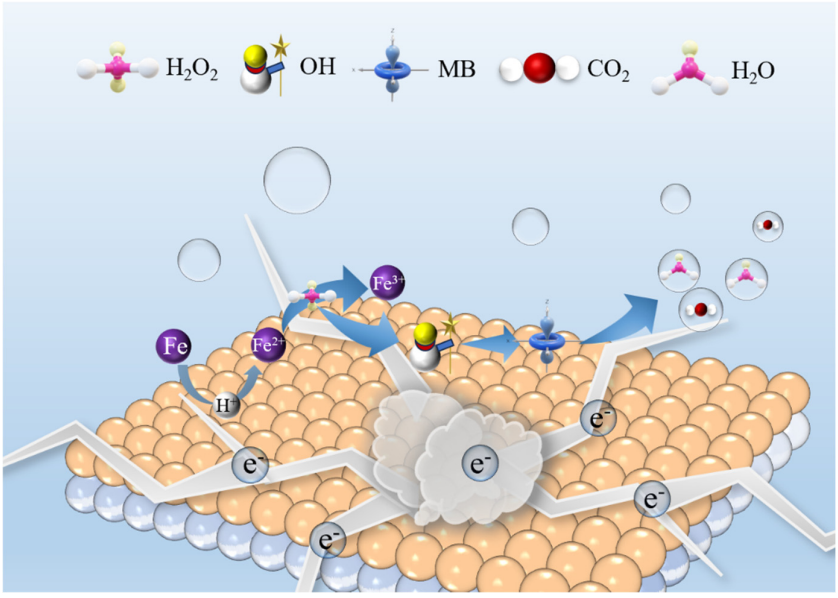


Figure 6. The mechanism diagram for $Fe_{80}P_{13}C_7$ catalytic degradation of MB.

In the $Fe_{80}P_{13}C_7$-catalyzed Fenton-like reaction, the valence state cycling of iron species is a core step driving the entire degradation process. The catalytic mechanism primarily relies on efficient electron transfer and regeneration between Fe^{2+} and Fe^{3+}: First, the spontaneously leached Fe^{2+} from $Fe_{80}P_{13}C_7$ reacts with H_2O_2, generating highly oxidative •OH through the classical Fenton pathway while being oxidized to Fe^{3+}. Subsequently, Fe^{3+} can further react with H_2O_2 (Fenton-like pathway), becoming reduced and regenerating Fe^{2+}. This closed-loop redox cycle of Fe^{2+}/Fe^{3+} continuously activates H_2O_2 molecules, ensuring stable and abundant generation of •OH, which fundamentally guarantees the efficient degradation of organic pollutants. The excellent cyclic stability of $Fe_{80}P_{13}C_7$ stems from its unique metastable structure as an MG that facilitates the smooth reduction of Fe^{3+}, allowing this critical regeneration step for Fe^{2+} to proceed efficiently and durably.

In summary, the reaction principle of $Fe_{80}P_{13}C_7$ catalyzing sH_2O_2 to produce •OH and thus degrading MB can be described as [35,36]:

$$Fe + H^{2+} \rightarrow Fe^{2+} + H_2 \quad (1)$$

$$Fe^{2+} + H_2O_2 \rightarrow Fe^{3+} + \bullet OH + OH^- \quad (2)$$

$$Fe^{3+} + H_2O_2 \rightarrow Fe^{2+} + \bullet OOH + H^+ \quad (3)$$

$$MB + \bullet OH \rightarrow CO_2 + H_2O \quad (4)$$

2.3. Limitations and Future Perspectives

Although our mechanistic interpretation is robustly supported by performance data and literature comparisons, we acknowledge that direct characterization of the surface chemical state remains an unfilled gap at the current stage. Consequently, we have es-

tablished a clear roadmap for subsequent research, with the immediate priority being the synthesis of new batches of materials followed by comprehensive surface analysis to ultimately confirm the surface self-regeneration process.

The $Fe_{80}P_{13}C_7$ MG developed in this study exhibits exceptional degradation efficiency for organic pollutants under acidic conditions. The optimal reaction pH of the system is 3.0, resulting in acidic effluent. Direct discharge of this effluent would cause a sharp decline in the pH of receiving water bodies, disrupt the balance of aquatic ecosystems, and potentially activate heavy metals in sediments, leading to secondary pollution. To address this, an alkaline reagent dosing unit (e.g., NaOH or $Ca(OH)_2$) can be installed after the catalytic oxidation unit to precisely adjust the effluent pH to the compliant range of 6.5–8.5. The iron-containing sludge generated during the neutralization process can be settled, separated, and evaluated for its feasibility as a building material additive or industrial raw material, thereby achieving waste resource utilization.

Although the $Fe_{80}P_{13}C_7$ MG demonstrates good stability in repeated experiments, potential challenges in long-term applications must be acknowledged. Firstly, in complex aqueous environments, anions (e.g., Cl^-, $CO_3{}^{2-}$) may occupy active sites through competitive adsorption while natural organic matter (e.g., humic acid) tends to form coverage layers on the catalyst surface, leading to physical deactivation. Secondly, although XRD analysis confirms the material maintains its amorphous structure post-reaction, prolonged operation or extreme conditions pose a risk of localized crystallization on the material surface, thereby reducing the density of highly active sites. Furthermore, the surface passivation layer formed during the reaction may thicken over extended operation, ultimately impeding electron transfer and mass transport efficiency. These potential mechanisms collectively represent critical factors affecting catalyst lifespan beyond physical surface cracking.

3. Experimental Materials and Methods

3.1. Preparation and Characterization of $Fe_{80}P_{13}C_7$ MG

The original $Fe_{80}P_{13}C_7$ ingot was synthesized through arc melting a mixture of high-purity Fe (99.99 wt.%), C (99.99 wt.%), and a pre-alloyed Fe-P ingot, which comprised 91.7 at.% Fe and 8.3 at.% P, under an atmosphere filled with purified Ar. Subsequently, the original $Fe_{80}P_{13}C_7$ ingot was remelted in a quartz tube using induction melting, followed by processing through a single-roller melt spinning system (roller tangent speed = 44 m/s) to produce an as-spun $Fe_{80}P_{13}C_7$ ribbon exhibiting a fully amorphous structure. This ribbon was initially vacuumed to 5×10^{-3} Pa before being filled with purified Ar gas. The resulting ribbon had a thickness of approximately 25 μm, a width of around 3 mm, and a length ranging from 20 to 30 cm. The $Fe_{80}P_{13}C_7$ metallic glass ribbons were prepared by the single-roller melt-spinning technique according to the method described by Chen et al. [40] with modifications.

The high-purity Fe, C, pre-alloyed Fe-P ingot, as well as industrial-grade Fe powder (1000 mesh; purity: $\geq$99.9 wt.%) utilized in this study was supplied by Jiangsu Jicui Antai Chuangming Advanced Energy Materials Research Institute Co., Ltd. (Changzhou, China).

In this study, the alterations in surface microstructure before and after degradation were examined using a field emission scanning electron microscope combined with energy dispersive spectroscopy (EDS). The experiment utilized a scanning electron microscope (SEM, Model SU8010, Hitachi, Tokyo, Japan) and an ultraviolet-visible spectrophotometer (UV5600i, Shimadzu Corporation, Kyoto, Japan) for sample characterization and analysis. Absorption spectra were recorded with a UV-visible spectrophotometer, focusing on the characteristic absorption peak of at 664 nm to quantitatively evaluate the concentration of MB solution.

3.2. Degradation Experiment

This study utilized Methylene Blue (MB, $C_{16}H_{18}ClN_3S$) obtained from Shanghai Aladdin Biochemical Technology Co., Ltd. (Shanghai, China); sodium hydroxide (NaOH, AR) sourced from China National Pharmaceutical Group Chemical Reagent Co., Ltd. (Beijing, China); concentrated sulfuric acid (H_2SO_4, 98%, AR) supplied by Shanghai Titan Technology Co., Ltd. (Shanghai, China); and hydrogen peroxide (H_2O_2, 30%) provided by Tianjin Yongda Chemical Reagent Co., Ltd. (Tianjin, China). Additionally, anhydrous ethanol and other chemicals were of analytical grade. The experiment employed a Shimadzu (Tokyo, Japan) UV5600i ultraviolet spectrophotometer to measure the absorbance of liquid samples collected during the degradation of dyes using catalysts.

Initially, a 250 mL solution of MB at a concentration of 50 mg/L was prepared. The dosage of the $Fe_{80}P_{13}C_7$ metallic glass catalyst was 1 g/L. A specific amount of H_2O_2 was added to this solution, and the pH was adjusted to between 2 and 9 using a 5% H_2SO_4 and NaOH solution while maintaining temperature control with a water bath. Subsequently, $Fe_{80}P_{13}C_7$ was introduced into the MB solution and stirred mechanically to ensure adequate contact between the catalyst and the solution. All experiments were conducted under conventional laboratory lighting conditions. At regular intervals, aliquots of 0.25 mL were taken from the MB solution and transferred into centrifuge tubes. Experimental parameters such as temperature, pH level, and H_2O_2 concentration were systematically varied in order to identify optimal conditions for MB degradation.

To quantitatively study the catalytic degradation performance of $Fe_{80}P_{13}C_7$, a pseudo-first-order kinetic model (Equation (5)) was used to fit the degradation curve, and the reaction rate constant (Equation (6)) was employed to assess the speed of the catalytic degradation reaction [39].

$$C_t/C_0 = \exp(-k_{obs}t) \quad (5)$$

$$k_{obs} = -\mathrm{In}\left(\frac{C_t}{C_0}\right)/t \quad (6)$$

In the equation presented above, C_0 and C_t denote the initial and instantaneous concentrations of the MB solution at time t, respectively; k_{obs} represents the kinetic reaction constant.

4. Conclusions

This study conducted an in-depth study on the performance and mechanism of $Fe_{80}P_{13}C_7$ MG in the catalytic degradation of MB, leading to the following core conclusions:

(1) $Fe_{80}P_{13}C_7$ exhibits excellent and stable catalytic performance in Fenton-like reactions. Its degradation rate not only surpasses that of FeSiB MG and commercial ZVI powder in benchmark experiments but also demonstrates significant advantages when compared with catalysts reported in recent literature, highlighting its potential as an efficient catalyst.

(2) $Fe_{80}P_{13}C_7$ possesses outstanding cyclic stability; after ten consecutive degradation cycles, its efficiency remains above 90% of the initial value. Scanning electron microscopy (SEM) analysis reveals that this stability is attributed to a unique surface "self-renewal" behavior. Specifically, cracks and corrosion features formed during the reaction effectively shed the passivation layer from the surface, continuously exposing high-activity fresh interfaces.

(3) Mechanistic analysis establishes that the reaction is predominantly governed by a closed cycle involving Fe^{2+}/Fe^{3+} species within the material itself. This cycle ensures continuous activation of H_2O_2 and generates a substantial amount of •OH radicals, thereby driving rapid and complete mineralization of pollutants.

In summary, $Fe_{80}P_{13}C_7$ MG represents an excellent Fenton-like catalyst characterized by high activity, long lifespan, and well-defined reaction mechanisms. This work lays a reliable foundation for its practical application in treating refractory organic wastewater.

Author Contributions: L.M.: Conceptualization, Methodology, Writing—original draft; K.Z.: Supervision, Project administration, Funding acquisition, Writing—review & editing; F.G.: Software, Formal analysis, Visualization; T.K.: Validation, Investigation, Writing—review & editing. All authors have read and agreed to the published version of the manuscript.

Funding: This work was supported by the National Natural Science Foundation of China (Grant No. 52174138).

Data Availability Statement: The data that support the findings of this study are available from the corresponding author upon reasonable request.

Conflicts of Interest: Authors Kun Zhang, Feilong Guo and Tiejun Kuang were employed by the company Jinneng Holding Coal Industry Group. The remaining authors declare that the research was conducted in the absence of any commercial or financial relationships that could be construed as a potential conflict of interest.

References

1. Liu, J.; Cheng, S.; Cao, N.; Geng, C.; He, C.; Shi, Q.; Xu, C.; Ni, J.; DuChanois, R.M.; Elimelech, M.; et al. Actinia-like multifunctional nanocoagulant for single-step removal of water contaminants. *Nat. Nanotechnol.* **2019**, *14*, 64–71. [CrossRef] [PubMed]
2. Selvaraj, V.; Karthika, T.S.; Mansiya, C.; Alagar, M. An over review on recently developed techniques, mechanisms and intermediate involved in the advanced azo dye degradation for industrial applications. *J. Mol. Struct.* **2021**, *1224*, 129195. [CrossRef]
3. Zhang, L.C.; Jia, Z.; Lyu, F.; Liang, S.X.; Lu, J. A review of catalytic performance of metallic glasses in wastewater treatment: Recent progress and prospects. *Prog. Mater. Sci.* **2019**, *105*, 100576. [CrossRef]
4. Ding, M.J.; Jia, D.X.; Yang, M.; Yu, Y.; Lin, G.C.; Zhang, X.L. A Detailed Insight into the Effects of Morphologies of Cerium Oxide on Fenton-like Reactions for Different Applications. *ChemPhysChem* **2023**, *24*, e202300211. [CrossRef]
5. Xing, M.; Xu, W.; Dong, C.; Bai, Y.; Zeng, J.; Zhou, Y.; Zhang, J.; Yin, Y. Metal sulfides as excellent co-catalysts for H_2O_2 decomposition in advanced oxidation processes. *Chem* **2018**, *4*, 1359–1372. [CrossRef]
6. Fu, F.; Dionysiou, D.D.; Liu, H. The use of zero-valent iron for groundwater remediation and wastewater treatment: A review. *J. Hazard. Mater.* **2014**, *267*, 194–205. [CrossRef]
7. Yang, Z.; Qian, J.; Yu, A.; Pan, B. Singlet oxygen mediated iron-based fenton-like catalysis under nanoconfinement. *Proc. Natl. Acad. Sci. USA* **2019**, *116*, 6659–6664. [CrossRef]
8. Li, X.F.; Liang, S.X.; Xi, X.W.; Jia, Z.; Xie, S.K.; Lin, H.C.; Hu, J.P.; Zhang, L.C. Excellent performance of $Fe_{78}Si_9B_{13}$ metallic glass for activating peroxymonosulfate in degradation of naphthol green B. *Metals* **2017**, *7*, 273. [CrossRef]
9. Liang, S.; Jia, Z.; Zhang, W.; Li, X.; Wang, W.; Lin, H.; Zhang, L. Ultrafast activation efficiency of three peroxides by $Fe_{78}Si_9B_{13}$ metallic glass under photo-enhanced catalytic oxidation: A comparative study. *Appl. Catal. B Environ.* **2018**, *221*, 108–118. [CrossRef]
10. Wang, J.; Liang, S.; Jia, Z.; Zhang, W.; Wang, W.; Liu, Y.; Lu, J.; Zhang, L. Chemically dealloyed Fe-based metallic glass with void channels-like architecture for highly enhanced peroxymonosulfate activation in catalysis. *J. Alloys Compd.* **2019**, *785*, 642–650. [CrossRef]
11. Jia, Z.; Wang, Q.; Sun, L.; Wang, Q.; Zhang, L.C.; Wu, G.; Luan, J.H.; Jiao, Z.B.; Wang, A.; Liang, S.X.; et al. Attractive in situ self-reconstructed hierarchical gradient structure of metallic glass for high efficiency and remarkable stability in catalytic performance. *Adv. Funct. Mater.* **2019**, *29*, 1807857. [CrossRef]
12. Liu, Q.; Liu, H.; Wang, M.; Zhang, Y.; Ma, Z.; Zhao, Y.; Yang, W. Effects of Ni substitution for Fe on magnetic properties of $Fe_{80-x}NixP_{13}C_7$ (x = 0–30) glassy ribbons. *J. Non-Cryst. Solids* **2017**, *463*, 68–71. [CrossRef]
13. Miao, F.; Wang, Q.; Di, S.; Yun, L.; Zhou, J.; Shen, B. Enhanced dye degradation capability and reusability of Fe-based amorphous ribbons by surface activation. *J. Mater. Sci. Technol.* **2020**, *53*, 163–173. [CrossRef]
14. Lassoued, A.; Li, J. Preparation, characterization and application of $Fe_{72}Cu_1Co_5Si_9B_{13}$ metallic glass catalyst in degradation of azo dyes. *J. Mater. Sci. Mater. Electron.* **2021**, *32*, 21727–21741. [CrossRef]
15. Luo, W.; Chen, Q.; Ji, L.; Peng, X.; Huang, G. Synergistic effect of various elements in $Fe_{41}Co_7Cr_{15}Mo_{14}C_{15}B_6Y_2$ amorphous alloy hollow ball on catalytic degradation of methylene blue. *J. Rare Earths* **2022**, *40*, 605–615. [CrossRef]

16. Zhang, P.; Zhu, Y.A.; Zhang, Y.; Lu, T.; Pan, Y. Heterogeneously structured FeCuBP amorphous–nanocrystalline alloy with excellent dye degradation efficiency. *Appl. Phys. A* **2021**, *127*, 330. [CrossRef]
17. Li, W.; Xiao, W.; Wang, G.; Wang, D.; Liu, M.; Wu, Y.; Wang, Z.; Aierken, A.; Chen, X.; Gao, C.; et al. Design and optimization of diatomic catalysts with synergistic effects for enhanced OER and ORR performance: Insights from a TM1TM2N8@BPN electrocatalyst. *J. Alloys Compd.* **2025**, *1031*, 180961. [CrossRef]
18. Zhan, X.; Weng, Z.; Ren, D.; Tong, X.; Liu, J.; Gao, R.; Shi, H. Dualatom catalysts beyond single-atom limitations: Mn/Co synergistic sites on crystalline g-C_3N_4 boosting photocatalysis. *J. Alloys Compd.* **2025**, *1030*, 180874. [CrossRef]
19. Yan, W.; Herzing, A.A.; Li, X.Q.; Kiely, C.J.; Zhang, W.X. Structural evolution of pd-doped nanoscale zero-valent iron (nZVI) in aqueous media and implications for particle aging and reactivity. *Environ. Sci. Technol.* **2010**, *44*, 4288–4294. [CrossRef]
20. Wei, F.; Zhang, J.; Yang, Z.; Liu, S.; Zhou, Z.; Li, F. Biomimetic degradation of perfluorinated acids by vitamin B_{12} with nano-zero-valent iron/nickel bimetal: Effects of their self-structure and coexisting substances. *Front. Environ. Sci. Eng.* **2025**, *19*, 18. [CrossRef]
21. Deng, F.; Vargas, H.O.; Rodriguez, O.G.; Qiu, S.; Yang, J.; Lefebvre, O. The synergistic effect of nickel-iron-foam and tripolyphosphate for enhancing the electrofenton process at circum-neutral pH. *Chemosphere* **2018**, *201*, 687–696. [CrossRef]
22. Liu, S.Q.; Xiao, B.; Feng, L.R.; Zhou, S.S.; Chen, Z.G.; Liu, C.B.; Chen, F.; Wu, Z.Y.; Xu, N.; Oh, W.C.; et al. Graphene oxide enhances the fenton-like photocatalytic activity of nickel ferrite for degradation of dyes under visible light irradiation. *Carbon* **2013**, *64*, 197–206. [CrossRef]
23. Montaner, M.B.; Hilton, S.T. Recent advances in 3D printing for continuous flow chemistry. *Curr. Opin. Green Sustain. Chem.* **2024**, *47*, 100923. [CrossRef]
24. Dory, H.; Petit, E.; El-Sayegh, S.; Badouric, L.; Castro, V.; Bechelany, M.; Voiry, D.; Miele, P.; Lajaunie, L.; Salameh, C. Monolith Catalyst Design by Combining 3D Printing and Atomic Layer Deposition: Toward Green Palladium-Catalyzed Cross-Coupling Reactions. *Adv. Eng. Mater.* **2025**, *24*, 202401546. [CrossRef]
25. Lange, A.; Arwish, S.; Rensonnet, A.; Elamin, K.; Abdurrokhman, I.; Wojnarowska, Z.; Rosenwinkel, M.; Malherbe, C.; Schoenhoff, M.; Zehbe, K.; et al. 3D Printable Polymer Electrolytes for Ionic Conduction based on Protic Ionic Liquids. *ChenPhysChem* **2025**, *26*, 202400849. [CrossRef]
26. Yang, W.; Wang, Q.; Li, W.; Xue, L.; Liu, H.; Zhou, J.; Mo, J.; Shen, B. A novel thermal-tuning Fe-based amorphous alloy for automatically recycled methylene blue degradation. *Mater. Des.* **2019**, *161*, 136–146. [CrossRef]
27. Hou, L.; Wang, Q.; Fan, X.; Miao, F.; Yang, W.; Shen, B. Effect of Co addition on catalytic activity of FePCCu amorphous alloy for methylene blue degradation. *New J. Chem.* **2019**, *43*, 6126–6135. [CrossRef]
28. Ji, L.; Chen, J.; Zheng, Z.; Qiu, Z.; Peng, S.; Zhou, S.; Zeng, D. Excellent degradation performance of the $Fe_{78}Si_{11}B_9P_2$ metallic glass in azo dye treatment. *J. Phys. Chem. Solids* **2020**, *145*, 109546. [CrossRef]
29. Luo, X.; Li, R.; Zong, J.; Zhang, Y.; Li, H.; Zhang, T. Enhanced degradation of azo dye by nanoporous-copper-decorated Mg–Cu–Y metallic glass powder through dealloying pretreatment. *Appl. Surf. Sci.* **2014**, *305*, 314–320. [CrossRef]
30. Li, Z.; Qin, X.; Zhu, Z.; Zheng, S.; Li, H.; Fu, H.; Zhang, H. Cu-based metallic glass with robust activity and sustainability for wastewater treatment. *J. Mater. Chem. A* **2020**, *8*, 10855–10864. [CrossRef]
31. Chen, F.; Chen, X.; Zou, L.; Yao, Y.; Lin, Y.; Shen, Q.; Lavernia, E.J.; Zhang, L. Fabrication and mechanical behavior of bulk nanoporous Cu via chemical de-alloying of Cu–Al alloys. *Mater. Sci. Eng. A* **2016**, *660*, 241–250. [CrossRef]
32. Yin, X.; Wang, Q.; Duan, D.; Liu, S.; Wang, Y. Amorphous NiB alloy decorated by Cu as the anode catalyst for a direct borohydride fuel cell. *Int. J. Hydrogen Energy* **2019**, *44*, 10971–10981. [CrossRef]
33. Li, S.; Zhou, M.; Wu, H.; Song, G.; Jing, J.; Meng, N.; Wang, W. High-efficiency degradation of carbamazepine by the synergistic electro-activation and bimetals (FeCo@NC) catalytic-activation of peroxymonosulfate. *Appl. Catal. B Environ.* **2023**, *338*, 123064. [CrossRef]
34. Zhou, Y.; Wang, J. Degradation of cephalosporin C using MOF-derived Fe-Co bimetal in carbon cages as electro-fenton catalyst at natural pH. *Sep. Purif. Technol.* **2023**, *323*, 124388. [CrossRef]
35. Abdelfatah, A.M.; Fawzy, M.; Eltaweil, A.S.; El Khouly, M.E. Green synthesis of nano-zero-valent iron using ricinus communis seeds extract: Characterization and application in the treatment of methylene blue-polluted water. *ACS Omega* **2021**, *6*, 25397–25411. [CrossRef]
36. Chen, F.; Ding, J.; Guo, K.; Yang, L.; Zhang, Z.; Yang, Q.; Yang, Y.; Bao, Z.; He, Y.; Ren, Q. CoNi alloy nanoparticles embedded in metalorganic framework-derived carbon for the highly efficient separation of xenon and krypton via a charge-transfer effect. *Angew. Chem.* **2021**, *133*, 2461–2468. [CrossRef]
37. Xie, S.; Yan, Y.; Lai, S.; He, J.; Liu, Z.; Gao, B.; Javanbakht, M.; Peng, X.; Chu, P.K. Ni^{3+}-enriched nickel-based electrocatalysts for superior electrocatalytic water oxidation. *Appl. Surf. Sci.* **2022**, *605*, 154743. [CrossRef]
38. Zhang, L.; Qiu, L.; Zhu, Q.; Liang, X.; Huang, J.; Yang, M.; Zhang, Z.; Ma, J.; Shen, J. Insight into efficient degradation of 3,5-dichlorosalicylic acid by Fe-Si-B amorphous ribbon under neutral condition. *Appl. Catal. B Environ.* **2021**, *294*, 120258. [CrossRef]

39. Wang, Q.; Chen, M.; Shao, L.; Ge, Y.; Lin, P.; Chu, C.; Shen, B. Effects of structural relaxation on thedye degradation ability of FePC amorphous alloys. *J. Non-Cryst. Solids* **2019**, *525*, 119671. [CrossRef]
40. Chen, Q.; Qi, Z.G.; Feng, Y.; Liu, H.Z.; Wang, Z.X.; Zhang, L.C.; Wang, W.M. Insight into fast catalytic degradation of neutral reactive red 195 solution by FePC glassy alloy: Fe release and OH generation. *J. Mol. Liq.* **2022**, *364*, 120058. [CrossRef]
41. Qu, J.; Xu, Y.; Zhang, X.; Sun, M.; Tao, Y.; Zhang, X.; Zhang, G.; Ge, C.; Zhang, Y. B-all milling-assisted preparation of N-doped biochar loaded with ferrous sulfide as persulfate activator for phenol degradation: Multiple active sites-triggered radical/non-radical mechanism. *Appl. Catal. B Environ.* **2022**, *316*, 121639. [CrossRef]
42. Yang, C.; Zhang, C.; Chen, Z.J.; Li, Y.; Yan, W.-Y.; Yu, H.-B.; Liu, L. Three-Dimensional Hierarchical Porous Structures of Metallic Glass/Copper Composite Catalysts by 3D Printing for Efficient Wastewater Treatments. ACS Appl. *Mater. Interfaces* **2021**, *13*, 7227–7237. [CrossRef] [PubMed]
43. Wang, X.; Zhang, Q.; Liang, S.X.; Jia, Z.; Zhang, W.; Wang, W.; Zhang, L.C. Fe-Based Metallic Glasses and Dyes in Fenton-Like Processes: Understanding Their Intrinsic Correlation. *Catalysts* **2020**, *10*, 48. [CrossRef]
44. Zuo, M.; Yi, S.; Choi, J. Excellent dye degradation performance of FeSiBP amorphous alloys by Fenton-like process. *J. Environ. Sci.* **2021**, *105*, 116–127. [CrossRef]
45. Chen, Q.; Yan, Z.; Zhang, H.; Zhang, L.C.; Ma, H.; Wang, W.; Wang, W. High MB Solution Degradation Efficiency of FeSiBZr Amorphous Ribbon with Surface Tunnels. *Materials* **2020**, *13*, 3694. [CrossRef]

Disclaimer/Publisher's Note: The statements, opinions and data contained in all publications are solely those of the individual author(s) and contributor(s) and not of MDPI and/or the editor(s). MDPI and/or the editor(s) disclaim responsibility for any injury to people or property resulting from any ideas, methods, instructions or products referred to in the content.